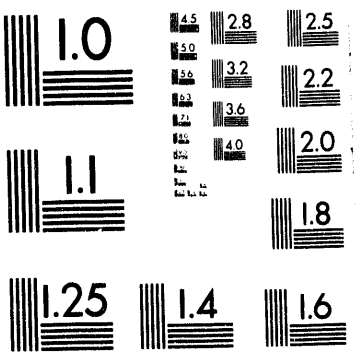
1.0
1.1
1.25
1.4
1.6
1.8
2.0
2.2
2.5
2.8
3.2
3.6
4.0
4.5
5.0
5.6

1 of 1

2

Conf-940391--2

UCRL-JC-116506
PREPRINT

Performance of Adaptive Optics at Lick Observatory

S. Olivier, J. An, K. Avicola, H. Bissinger
J. Brase, H. Friedman, D. Gavel, E. Johansson,
C. Max, K. Waltjen, W. Fisher and W. Bradford

This paper was prepared for submittal to the
Astronomical Telescopes & Instrumentation
for the 21st Century
Kona, Hawaii
March 13-18, 1994

March 1994

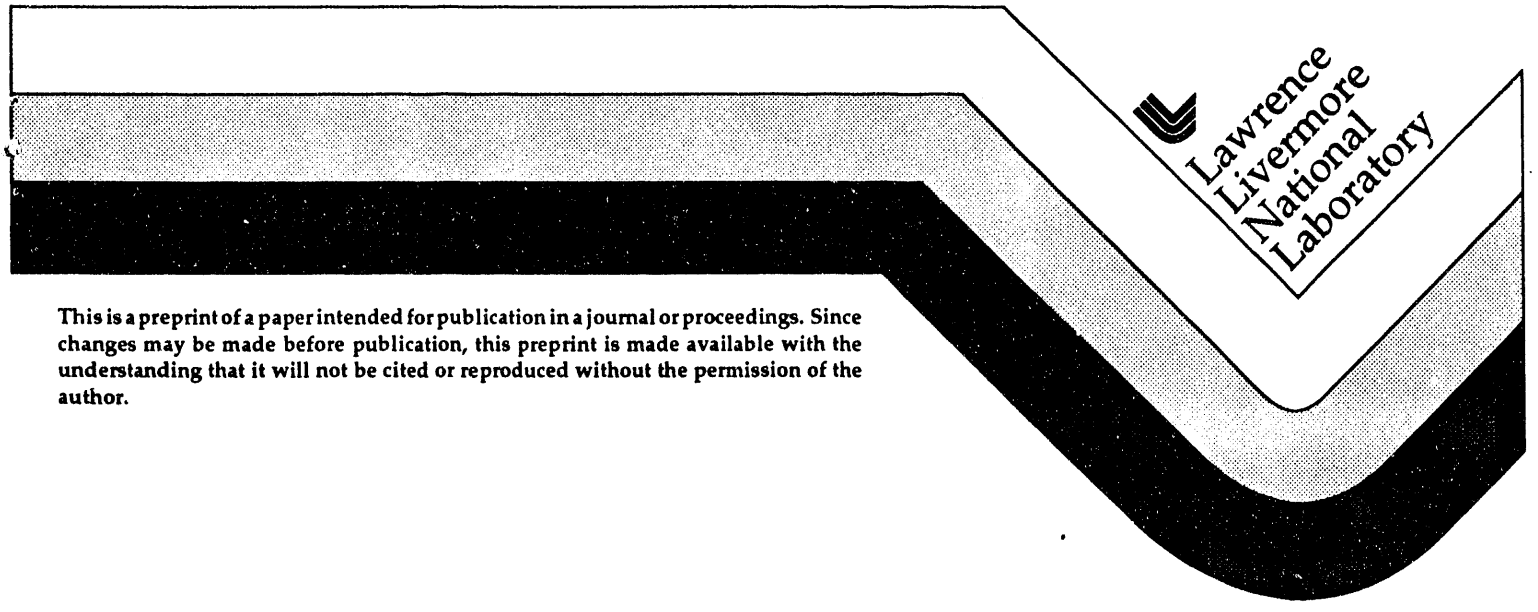

DISCLAIMER

Performance of adaptive optics at Lick Observatory

Scot S. Olivier, Jong An, Kenneth Avicola, Horst D. Bissinger,
James M. Brase, Herbert W. Friedman, Donald T. Gavel,
Erik M. Johansson, Claire E. Max, Kenneth E. Waltjen

Lawrence Livermore National Laboratory, Livermore, CA 94550.

William Fisher

Lockheed Palo Alto Research Center, Palo Alto, CA 94304.

William Bradford

Physics Department, University of California, Santa Cruz, CA 95064

ABSTRACT

A prototype adaptive optics system has been developed at Lawrence Livermore National Laboratory (LLNL) for use at Lick Observatory. This system is based on an ITEK 69-actuator continuous-surface deformable mirror, a Kodak fast-framing intensified CCD camera, and a Mercury VME board containing four Intel i860 processors. The system has been tested using natural reference stars on the 40-inch Nickel telescope at Lick Observatory yielding up to a factor of 10 increase in image peak intensity and a factor of 6 reduction in image full width at half maximum (FWHM). These results are consistent with theoretical expectations.

In order to improve performance, the intensified CCD camera will be replaced by a high-quantum-efficiency low-noise fast CCD camera built for LLNL by Adaptive Optics Associates using a chip developed by Lincoln Laboratory, and the 69-actuator deformable mirror will be replaced by a 127-actuator deformable mirror developed at LLNL. With these upgrades, the system should perform well in median seeing conditions on the 120-inch Shane telescope for observing wavelengths longer than ~ 1 μm and using natural reference stars brighter than $m_R \sim 10$ or using the laser currently being developed at LLNL for use at Lick Observatory to generate a sodium-layer reference star.

1. INTRODUCTION

The resolution of astronomical images obtained from the ground is limited by aberrations associated with atmospheric turbulence to angular sizes much larger than the theoretical diffraction limit of large telescopes. Babcock[1] suggested that these aberrations could be sensed and corrected in real time using an adaptive optics system thereby producing diffraction-limited images. This concept is now being applied by a number of groups to improve astronomical images.

A prototype adaptive optics system has been developed at LLNL for use at Lick Observatory. This system is being tested on the 40-inch Nickel telescope using natural reference stars, and an upgraded version of the system is planned for the 120-inch Shane telescope where it can use a sodium-layer laser reference star that will be generated by a Nd-YAG-pumped dye laser currently being developed at LLNL.

In this paper, we will describe the prototype adaptive optics system and present results from the engineering tests. The test results will be compared with theory, and will be used along with the results from an atmospheric monitoring program which was carried out at Lick over the last year, to predict the performance of planned upgraded versions of the system.

2. ATMOSPHERIC CHARACTERIZATION

In order to predict how well an adaptive optics system will perform at a particular site, it is necessary to know what the atmospheric conditions at the site are. An atmospheric characterization program has been carried out at Lick Observatory on the 40-inch Nickel telescope over the last year using a variety of methods to measure the coherence length (r_0), the coherence time (τ_0), and the coherence angle (θ_0).

Two different types of measurements have been used to determine the atmospheric parameters.

The first type of measurement is speckle interferometry or short-exposure imaging using a CCD camera and a fast shutter. This system was used to take a series stellar images with exposure times between 1 and 100 ms and at wavelengths of 0.55, 0.7, 0.85, and 1.0 μm.

The atmospheric coherence length can be found from a series of short-exposure images by fitting the theoretical ensemble-average short-exposure modulation transfer function to the data[2]. A number of values for r_0 calculated using this method are shown in Figure 1a.

The atmospheric coherence time can be estimated from several series of short-exposure images taken at different exposure times by examining the high-spatial-frequency part of the power spectrum[3]. Several estimates of τ_0 using this method are shown in Figure 1b.

The atmospheric coherence angle can be found from a series of short-exposure images of double stars by calculating the ensemble-average cross-correlation for the speckle interferograms from each of the stars[4]. Several values of θ_0 calculated using this method are shown in Figure 1c.

The second type of measurement is wavefront tilt sensing using an 8×8 Hartmann lenslet array imaging onto a fast-framing intensified CCD camera. This system was used to measure stellar wavefront tilts at 1 kHz for a period of 1 second and at a wavelength of $\sim 0.6\mu$m.

The atmospheric coherence length can be found from the wavefront tilt data by calculating the root-mean-square (rms) differential angle of arrival from adjacent subapertures of the Hartmann array[5]. Several values for r_0 calculated using this method are shown in Figure 1a.

The atmospheric coherence time can be found from the wavefront tilt data by first reconstructing the wavefront phase, then computing the phase temporal power spectrum and computing the frequency for which the integral of the power spectrum from that frequency to infinity yields 1 radian of rms phase error. Several values of τ_0 using this method are shown in Figure 1b.

From Figure 1a, it can be seen that if the median value of r_0 from each night is given equal weight, then the median value of r_0 for the year is $\sim$ 6 cm. However there is a definite seasonal variation with a median r_0 of $\sim$ 4 cm in the Winter and Spring, and a median r_0 of $\sim$ 7 cm in the Summer and Fall. From Figure 1b, it can be seen that median value of τ_0 is $\sim$ 6

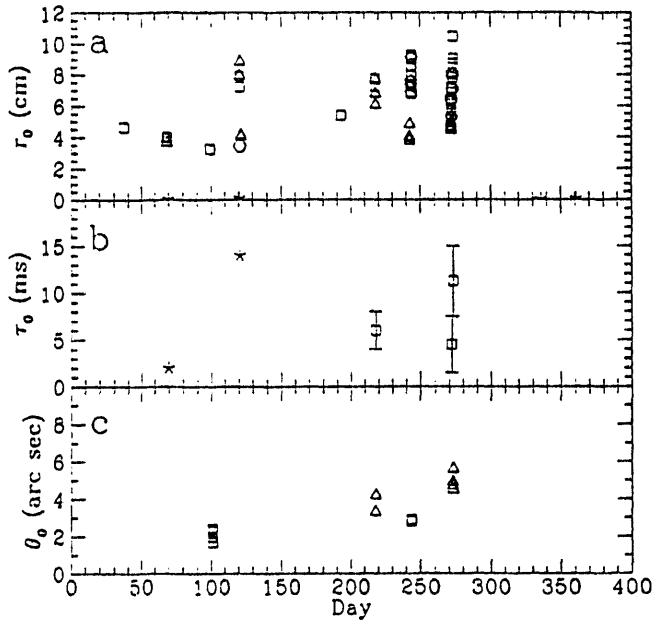

Figure 1 – Atmospheric coherence length (a), coherence time (b), and coherence angle (c) at $\lambda = 0.55$ μm measured at the Lick Observatory 40-inch Nickel telescope during 1993. The open symbols are values calculated using speckle data (triangles: $\lambda = 0.55$ μm, squares: $\lambda = 0.7$ μm, pentagons: $\lambda = 0.85$ μm, hexagons: $\lambda = 1.0$ μm), while the closed stars are values calculated using wavefront tilt data. Values calculated from data taken at wavelengths other than 0.55 μm has been scaled by $(0.55\ \mu\text{m}/\lambda)^{1.2}$.

ms, and from Figure 1c, it can be seen that the median value of of θ_0 is ~ 3 arc seconds. These median values will be used in section 7 to predict the upgraded system performance.

3. LICK ADAPTIVE OPTICS SYSTEM DESCRIPTION

The prototype Lick adaptive optics system uses a Hartmann wavefront sensor with a rectangular array of 48 subapertures in the clear aperture of the telescope. Images from the lenslets are recorded using a Kodak intensified CCD camera. This camera has a large format (192 × 239 pixels), a high frame rate (1 kHz), but a low quantum efficiency. In the future, the Kodak camera will be replaced with a high-quantum-efficiency low-noise fast CCD camera currently being built for LLNL by Adaptive Optics Associates using a 64 × 64 chip developed by Lincoln Laboratory.

The wavefront tilt data recorded by the wavefront sensor is used to reconstruct the wavefront phase. The wavefront reconstructor is based on four Intel i860 chips on a Mercury VME board and is controlled by a Unix workstation.

The reconstructed wavefront phase is used to control a deformable mirror built by Itek for Lockheed with a rectangular array of 69 actuators.

The Lick adaptive optics system also contains a separate tip-tilt system both to conserve the dynamic range of the deformable mirror and because when the wavefront information is obtained from a laser reference star, the tip-tilt information must be obtained separately from

a natural star. The tip-tilt system is based on an avalanche photodiode quad-cell sensor and a small (2.5 cm) tip-tilt mirror with an analog controller.

A more detailed description of the prototype Lick adaptive optics system design is given in another paper in this proceedings[6].

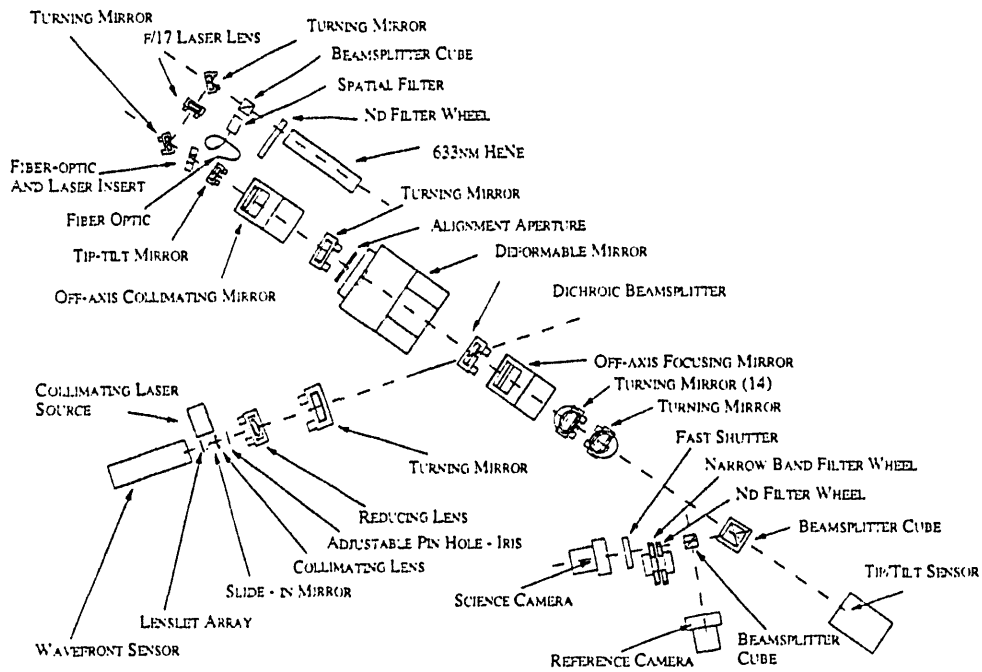

Figure 2 – Prototype Lick adaptive optics system optical schematic.

The optical schematic for the prototype Lick adaptive optics system is shown in Figure 2. Light from the telescope enters from the upper left on the diagram and hits a turning mirror, the tip-tilt mirror, an off-axis collimating mirror, another turning mirror, and then the deformable mirror. The light then hits a dichroic beamsplitter that reflects the light shorter than $\lambda = 0.6$ μm to the wavefront sensor leg which consists of a turning mirror, a reducing lens, a collimating lens, the lenslet array, and finally the wavefront sensor camera. The light longer than $\lambda = 0.6$ μm passes through the dichroic beamsplitter to the science camera leg which consists of an off-axis focussing mirror, two turning mirrors, and a beamsplitter cube that sends half the light to the tip-tilt sensor and half the light to the science camera.

The actual optical layout and a description of the calibration procedures is given in another paper in this proceedings[6].

4. ADAPTIVE OPTICS ENGINEERING TEST RESULTS

An engineering test of the prototype Lick adaptive optics system was conducted on Feb. 28, 1994. Open and closed-loop imaging data for the star Alpha Aurigae at wavelengths of 0.7 μm and 0.85 μm are shown in Figure 3. The open-loop images were taken with an exposure time of 10 s, while the closed-loop images were taken with an exposure time of 1 s. The data have been scaled to account for the difference in the exposure time and it has been verified that the open and

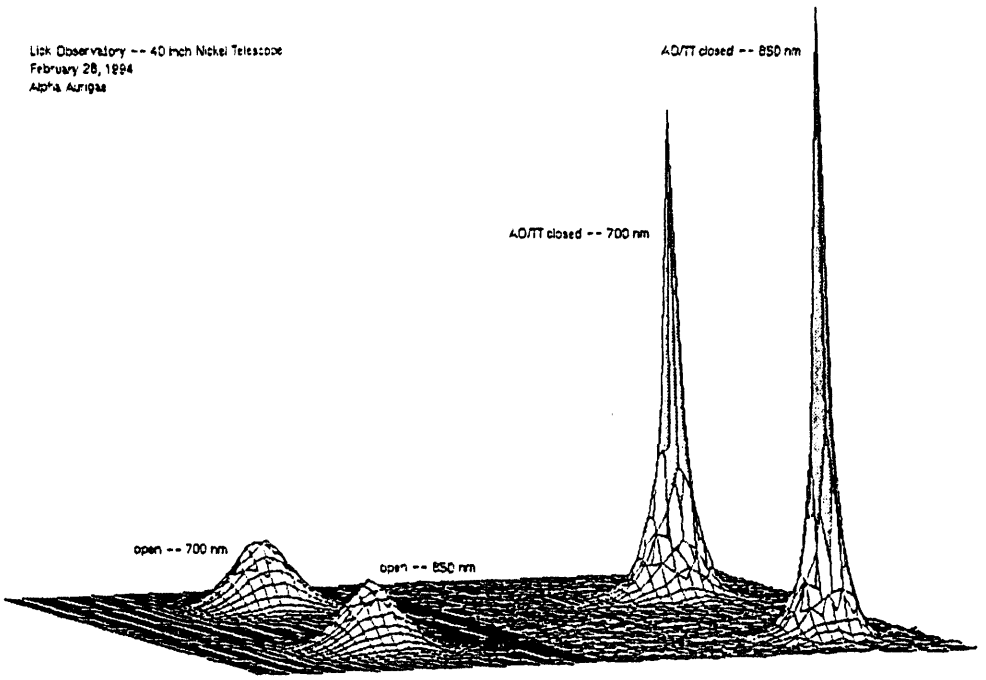

Figure 3 – Images of Alpha Aurigae with and without adaptive optics compensation. These images were obtained during an engineering test of the prototype Lick adaptive optics system on Feb. 28, 1994.

closed-loop images contain the same amount of light. In order to improve clarity, the data have also been scaled so that the peaks of the open-loop images are the same for both wavelengths.

The radially averaged intensities for the open and closed-loop images of Alpha Aurigae are shown in Figure 4. From the data shown in Figure 4, it is possible to calculate the FWHM of the images along with θ_{50} and θ_{80} (the angles that contain 50% and 80% of the light respectively). These values are given in Table 1a. The diffraction-limited FWHM is also given for comparison.

The ratio of the open-loop to diffraction-limited FWHM is a measure of D/r_0. If the data are scaled so that the peak of the open-loop image is equal to $(r_0/D)^2$, then the peak intensities of the data are equal to the Strehl ratios. This scaling has been applied in Figure 4, and the results for the Strehl ratios are given in Table 1b.

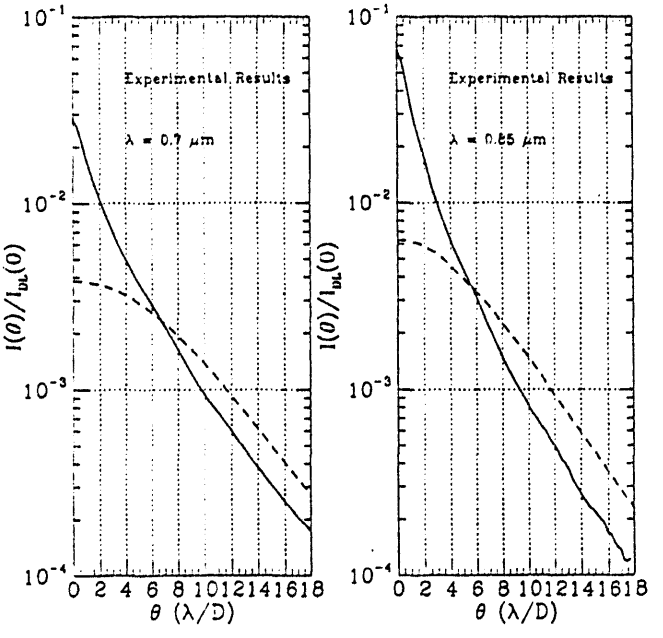

Figure 4 – Radially averaged image data from Alpha Aurigae with and without adaptive optics compensation.

TABLE 1a. Alpha Aurigae image angular statistics with and without adaptive optics compensation.

Data set	diff. lmtd. FWHM	FWHM	FWHM decrs.	incrs. from d. l.	θ_{50}	θ_{50} decrs.	θ_{80}	θ_{80} decrs.
0.7 μm								
open	0.144"	2.34"		16.3	2.73"		4.52"	
closed	0.144"	0.390"	6.0	2.7	1.73"	1.58	3.28"	1.38
0.85 μm								
open	0.175"	2.20"		12.6	2.84"		4.76"	
closed	0.175"	0.351"	6.29	2.0	1.48"	1.92	2.97"	1.60

TABLE 1b. Alpha Aurigae image peak intensity statistics with and without adaptive optics compensation.

Data set	D/r_0	Strehl ratio	Strehl incrs.
0.7 μm			
open	16.3	0.0038	
closed	16.3	0.028	7.4
0.85 μm			
open	12.6	0.0063	
closed	12.6	0.067	10.6

During this engineering test, open and closed-loop wavefront tilt data were also collected for the star Alpha Bootes. These data are shown in Figure 5. The frequency where the open and closed-loop tilt power spectra cross is a measure of the system bandwidth. From this data, the system bandwidth is found to be $\sim$ 30 Hz, which is consistent with the analysis of the control system.[6]

The wavefront tilt data were used to calculate r_0 from the differential angle of arrival, and the result was $r_0(\lambda = 0.55\mu\text{m}) = 4.7$ cm. This value is consistent with the values of D/r_0 given in Table 1b assuming that r_0 scales with $\lambda^{1.2}$ as predicted by Kolmogorov theory.

5. COMPARISON TO THEORY

There are four main sources of error inherent in adaptive optics compensation. Each of these errors is introduced because of a difference between the estimate of the reference wavefront and the actual wavefront of the astronomical object being imaged. To first order, we can treat the errors from each of the four sources as being uncorrelated. Therefore, the square of the residual wavefront phase error will be given by the quadrature sum:

$$\sigma_{wf}^2 = \sigma_m^2 + \sigma_f^2 + \sigma_s^2 + \sigma_a^2. \tag{1}$$

where σ_m is the measurement error, σ_f is the fitting error, σ_s is the servo error, and σ_a is the anisoplanatic error.

The measurement error is due to the inability of the wavefront sensor to accurately measure the shape of the reference wavefront in the presence of noise. The fitting error is due to the inability of the adaptive optics system to respond to the high-spatial-frequency variations of

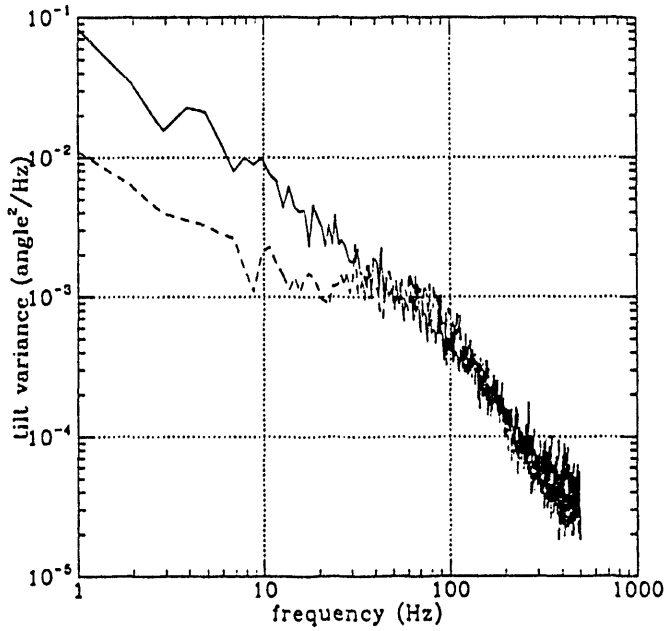

Figure 5 – Wavefront tilt power spectra from Alpha Bootes with and without adaptive optics compensation. These data were obtained during an engineering test of the prototype Lick adaptive optics system on Feb. 28, 1994.

the atmosphere. The servo error is due to the inability of the control loop to respond to the high-temporal-frequency variations of the atmosphere. The anisoplanatic error is due to the difference in the atmospheric aberrations between the wavefront reference and the object being imaged.

In the limit of small residual wavefront phase error, the Strehl ratio is given by

$$S = \exp(-\sigma_{wf}^2). \tag{2}$$

Note that although equation (2) is a good approximation to the long-exposure or uncompensated Strehl ratio only for $\sigma_{wf}^2 \lesssim 1$ rad^2, it is a good approximation to the Strehl ratio after compensation by an adaptive optics system with ~ 100 degrees of out to $\sigma_{wf}^2 \sim 7$ rad^2 (i.e., down to Strehl ratios of $\sim 10^{-3}$).[7]

Since the engineering test described in the previous section was conducted using a single bright star, the measurement and anisoplanatic errors were small, so they will be neglected in this analysis.

The fitting error can be expressed as[8]

$$\sigma_f^2 = \mu(d/r_0)^{5/3}, \tag{3}$$

where d is the actuator spacing mapped to the entrance aperture of the telescope, and μ is a coefficient that depends on the deformable mirror geometry and influence function. For the ITEK mirror we are using, $\mu \approx 0.27$.

The servo error can be expressed as[9]

$$\sigma_s^2 = \beta(f_0/f)^{5/3} \tag{4}$$

where f is the servo bandwidth defined as the frequency at which the spectrum of the control loop crosses the -3 dB point, and β is a coefficient that depends on the spectral shape of the control loop transfer function. For the control loop we are using, $\beta \approx 1.0$.

The formula for servo bandwidth error is valid only in the limit of very large D/r_0. For smaller values of D/r_0, the servo bandwidth error will be smaller than the value given by equation (4). This is essentially due to the fact that for smaller values of D/r_0, the atmosphere introduces a smaller amount of wavefront phase error, even before any correction is attempted.

Expressions for the Strehl ratio as a function of servo bandwidth that include the dependence on D/r_0 have been derived by Tyler[10]. Tyler's numerical results for the Strehl ratio in the presence of a finite servo bandwidth can be approximated by the expression $S = \exp[-(f_0'/f)^{5/3}]$, where f_0' is the effective atmospheric coherence frequency defined by

$$f_0' \equiv f_0/\left[1 + 1/\log_{10}(D/r_0)\right]. \tag{5}$$

Using equations (1)-(5) and the measured values of D/r_0, f, it is possible to compute a value for f_0 that gives the measured Strehl ratios for the image data presented in the previous section. These quantities are given in Table 2. along with the individual wavefront error terms. Since the value of f_0 was not measured, this is not a rigorous proof of the theory, but it does give a consistency check if the calculated values of f_0 are in a reasonable range.

TABLE 2. Predicted error terms and Strehl ratios for Alpha Aurigae image data after adaptive optics compensation.

Data set	D/r_0	f (Hz)	f_0 (Hz)	σ_f^2 (rad^2)	σ_s^2 (rad^2)	Strehl ratio
0.7 μm	16.3	30	99	0.88	2.73	0.028
0.85 μm	12.6	30	90	0.58	2.12	0.067

From Table 2, it can be seen that the values of f_0 that are consistent with the measured Strehl ratios correspond to $\tau_0(\lambda = 0.55\mu\text{m}) = 6.6$ and 7.6 ms. These values are consistent with those expected based on the atmospheric measurements presented in Section 2.

A more detailed theoretical model of the Alpha Aurigae imaging data can be constructed by modeling the adaptive optics system as a spatial filter on the wavefront phase spatial power

spectrum.[7] This analysis allows one to compute the expected MTF and PSF for the system. Figure 6 shows the theoretical open and closed-loop PSFs calculated using the measured values of $D/r0$. The width of the spatial filter was chosen in each case to match the measured Strehl ratios. Comparing Figures 6 and 4, it can be seen that there is good agreement in the details of the experimental and theoretical PSFs.

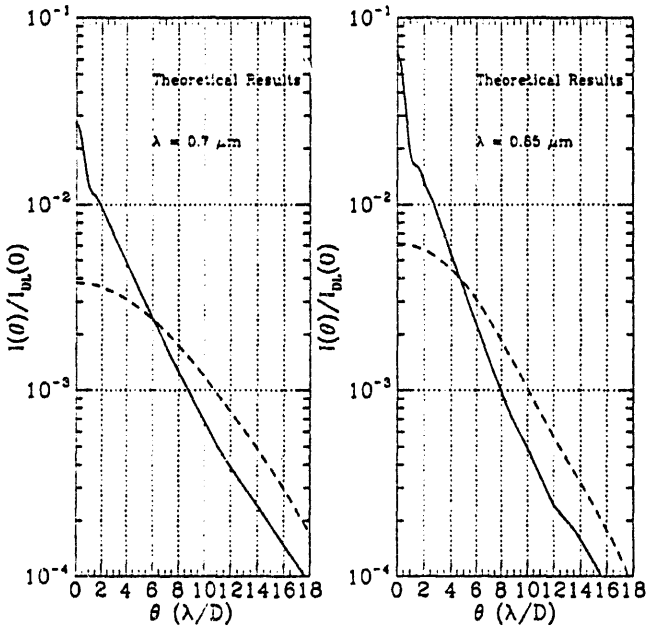

Figure 6 – Theoretical open and closed-loop PSFs using a spatial filter model for the adaptive optics system. The width of the spatial filter has been set so that the closed-loop results give the measured Strehl ratios. These theoretical PSFs are in good agreement with the measured PSFs shown in Figure 4.

6. PERFORMANCE PREDICTIONS

Using the measured median values of the atmospheric parameters and the measured system control loop bandwidth, it is possible to predict the performance of the Lick adaptive optics system on both the 40-inch Nickel and the 120-inch Shane telescope. In order to improve the magnitude limit of the system, a high-quantum-efficiency low-noise fast CCD camera will be used instead of the current intensified CCD camera, so in the following analysis the upgraded camera will be assumed.

Figure 7 shows the expected performance of the Lick adaptive optics system on the 40-inch Nickel telescope at several different observing wavelengths as a function of the magnitude of the reference star. For bright stars, the system will be limited by both the fitting and the servo error. For dimmer stars, the system is also limited by the measurement error. In this regime, servo bandwidth has been chosen to give the optimal relationship between servo error and measurement error.[11]

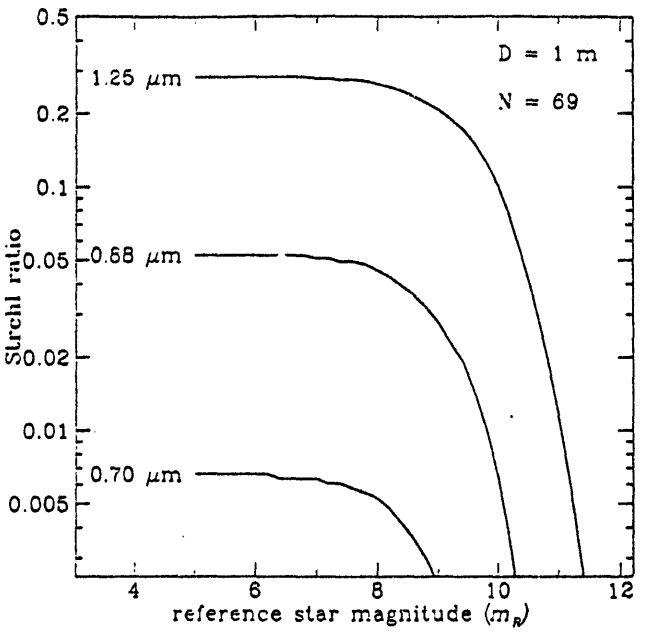

Figure 7 – Expected performance of the Lick adaptive optics system on the 40-inch Nickel telescope for median atmospheric conditions

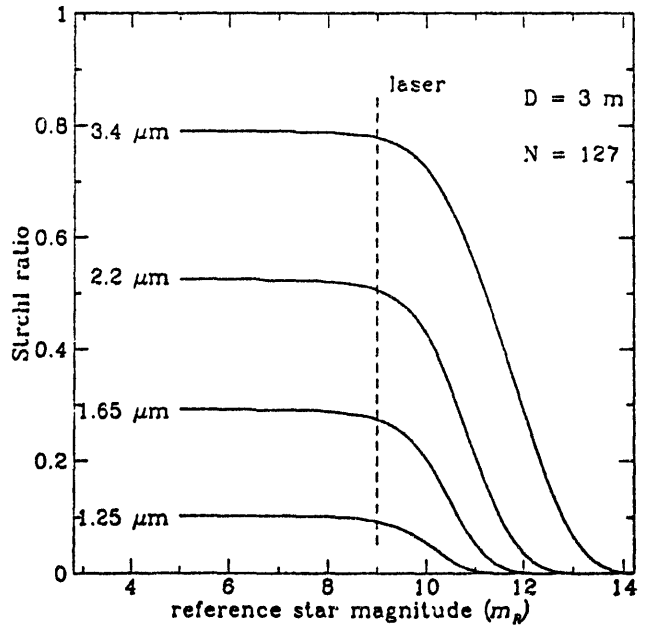

Figure 8 – Expected performance of the Lick adaptive optics system using the 127-actuator deformable mirror on the 120-inch Shane telescope for median atmospheric conditions. The dashed line marks the expected performance when the system is operated using the laser reference star.

In order to improve the fitting error and to make the system more robust, when the system is operated on the 120-inch Shane telescope, the old 69-actuator deformable mirror will be

replaced by a new 127-actuator deformable mirror developed at LLNL. The expected performance of the Lick adaptive optics system (with the 127-actuator deformable mirror) on the 120-inch Shane telescope is shown in Figure 8 as a function of the magnitude of the reference star for several different observing wavelengths.

Figure 8 also shows the expected performance of the Lick adaptive optics system when it is operated using a sodium-layer laser reference star that will be generated by a Nd-YAG-pumped dye laser currently being developed at LLNL.[12]

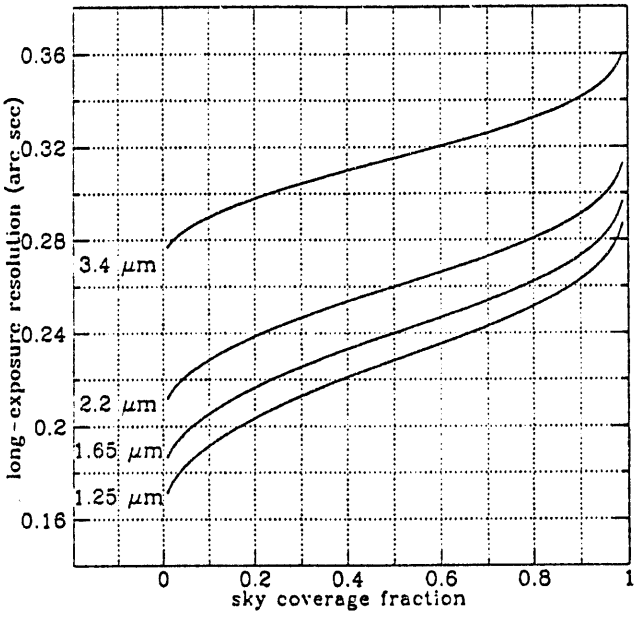

Figure 9 – Expected long-exposure resolution for the Lick adaptive optics system when the system uses the laser reference star to correct the short-exposure images.

The performance of the Lick adaptive optics system using the laser reference star shown in Figure 8 does not include the degradation from tip-tilt since this must be corrected using a natural star. Figure 9 shows the expected long-exposure resolution from the Lick adaptive optics system, when the system uses the laser reference star to correct the short-exposure images, as a function of the sky coverage fraction. This performance has been calculated using the optimum values for the tilt reference star magnitude limit and the tilt system servo bandwidth.[13]

7. ACKNOWLEDGMENTS

Work performed under the auspices of the U.S. Department of Energy by Lawrence Livermore National Laboratory under Contract W-7405-Eng-48.

8. REFERENCES

1. H. W. Babcock, "Adaptive optics revisited," Science, **249**, 253-257 (1990).
2. D. Korff, "Analysis of a method for obtaining near-diffraction-limited information in the presence of atmospheric turbulence," J. Opt. Soc. Am., **63**, 971-980 (1973).

3. D.P. Karo and A.M. Schneiderman, "Speckle interferometry at finite spectral bandwidths and exposure times," J. Opt. Soc. Am., **68**, 480-485 (1978).

4. J. Vernin, G. Weigelt, J.-L. Caccia, and M. Müller, "Speckle lifetime and isplanicity determinations: direct measurements and derivation from turbulence and wind profiles," Astron. Astrophys., **243**, 553-558 (1991).

5. D. L. Fried, "Differential angle of arrival: Theory, evaluation, and measurement feasibility," Radio Sci., **10**, 71-76 (1975).

6. J. M. Brase, J. An, K. Avicola, H. D. Bissinger, H. W. Friedman, D. T. Gavel, B. Johnston, C. E. Max, S. S. Olivier, R. Presta, D. A. Rapp, J. T. Salmon, and K. E. Waltjen, "Adaptive optics at Lick Observatory: System architecture and operations," Proc. Soc. Photo-Opt. Instrum. Eng., **2201**, in press (1994).

7. D. T. Gavel and S. S. Olivier, "Simulation and analysis of laser guide star adaptive optics systems for the 8- to 10-meter-class telescopes," Proc. Soc. Photo-Opt. Instrum. Eng., **2201**, in press (1994).

8. D. L. Fried, J. Opt. Soc. Am., **55**, 1427 (1965).

9. D. P. Greenwood and D. L. Fried, "Power spectra requirements for wave-front-compensative systems," J. Opt. Soc. Am., **66**, 193-206 (1976).

10. G. A. Tyler, "Turbulence-induced adaptive-optics performance degredation: evaluation in the time domain," J. Opt. Soc. Am. A, **1**, 251-262 (1984).

11. S. S. Olivier, "Optimized performance of natural reference star adaptive optics systems," Astrophys. J., submitted (1994).

12. H. W. Friedman, T. Kuklo, J. N. Wong, R. H. Page, and G. R. Thompson, "Design of a fieldable laser system for a sodium guide star," Proc. Soc. Photo-Opt. Instrum. Eng., **2201**, in press (1994).

13. S. S. Olivier and D. T. Gavel, "Tip-tilt compensation for astronomical imaging," J. Opt. Soc. Am. A, **11**, 368-378 (1994).

DATE
FILMED
5/4/94
END